Journal of Engineering Mathematics (2005) 52: 167–184
DOI 10.1007/s10665-004-6451-1

Bifurcation analysis for shear localization in non-polar and micro-polar hypoplastic continua

WENXIONG HUANG, MOHAMMED HJIAJ and SCOTT W. SLOAN
School of Engineering, The University of Newcastle, Callaghan NSW 2308, Australia
(wh670@alinga.newcastle.edu.au)

Received 16 December 2003; accepted in revised form 15 November 2004

Abstract. In this paper, shear localization in granular materials is studied as a bifurcation problem based on a conventional (non-polar) and a micro-polar continuum description. General bifurcation conditions are formulated for a non-polar hypoplastic model and its micro-polar continuum extension. These conditions define stress, couple stress and density states at which weak discontinuity bifurcation may occur. The stress states for bifurcation are then compared with the peak stress states, which define a bounding surface for the accessible stress domain in the principal stress space. The results show that, in a micro-polar continuum description, the constitutive model may no longer be associated with weak discontinuity bifurcation.

Key words: bifurcation analysis, granular materials, hypoplasticity, micro-polar continuum, non-polar continuum

1. Introduction

Localized deformation, in the form of narrow shear zones known as shear bands, is a widely observed phenomenon in granular materials when a certain limit state is approached. Analysis of shear localization can give some insight into the failure mechanism of granular materials and may provide further understanding for constitutive modelling of inelastic behavior.

Following the pioneering work of Rice [1] and Rudnicki and Rice [2], the phenomenon of shear localization has often been directly associated with the weak discontinuity bifurcation properties of constitutive models. The onset of shear localization was understood "in the sense that the constitutive relations may allow the homogeneous deformation of an initially uniform material to lead to a bifurcation point, at which non-uniform deformation can be incipient in a planar band under conditions of continuing equilibrium and continuing deformation outside the zone of localization" [2]. The technique of bifurcation analysis has been widely used to predict the occurrence of shear localization [3, 4].

It is well known that constitutive models developed within the framework of conventional continuum theory are limited to modelling pre-bifurcation behavior. Due to the lack of an internal length, these models cannot capture the thickness of the localized zones. As a result, numerical modelling of post-bifurcation behavior suffers from severe mesh-dependency.

Consideration of the relevant micro-mechanics leads to the application of enhanced continuum theory, including non-local theory, higher-gradient theory and micro-polar continuum theory, in the macro-description of granular materials. These theories introduce a characteristic length, which regularizes the failure process with non-local effects. In particular, recent work has established links between inter-granular contacts and the continuum quantities such as stress and couple stress [5, 6]. Thus micro-polar continuum theory has become a suitable framework for macro-description of granular media. The theory has been used to study shear

localization in granular materials by Mühlhaus [7], de Borst [8], Dietsche *et al.* [9] and Ehlers and Volk [10] who adopted an elastoplastic approach, and by Tejchman [11], Tejchman and Bauer [12], Bauer and Huang [13], Tejchman and Gudehus [14] and Huang and Bauer [15] who adopted a hypoplastic approach. It is widely accepted that post-bifurcation behavior can be well captured by micro-polar continuum models. Numerical results for shearing of a granular layer between two parallel plates show that a localized shear zone of finite thickness can be obtained, which is mesh-independent provided that the element size is small enough [14, 15].

An open question with the micro-polar continuum description of granular materials is whether shear localization will occur in a homogeneous deforming specimen in the form of weak discontinuity bifurcation (as is the case in a conventional continuum description). This paper focuses on bifurcation analysis of constitutive models developed for cohesionless granular materials using a conventional (non-polar) continuum approach and a micro-polar continuum approach. The non-polar hypoplastic model proposed by Gudehus [16] and Bauer [17], and its micro-polar continuum extension formulated by Huang *et al.* [18], are employed for this purpose. In these non-polar and micro-polar models, the void ratio is incorporated as a measurement of density. This allows the stationary state (the so-called critical state) to be described and the pressure- and density-dependent behavior to be captured for a wide range of stress and density levels with a single set of constitutive constants.

Hypoplastic constitutive models belong to a category known as incrementally nonlinear models. Bifurcation analysis of non-polar models of this type was first discussed by Kolymbas [19] and Chambon and Desrues [20]. A more general analysis can be found in [21,22]. Bauer and Huang [23] and Bauer [24] discussed the pressure and density effects in bifurcation and shear localization. Wu and Sikora [25] and Wu [26] presented a bifurcation surface in principal-stress space for a density-independent hypoplastic model. Fewer results are known for bifurcation analysis of micro-polar continuum models. Some early results can be found in, for instance, [9,27].

In this paper, a general criterion for bifurcation is first derived for the non-polar hypoplastic continuum. By extending the concept of a weak discontinuity in the micro-polar continuum, a similar bifurcation criterion is formulated for the micro-polar hypoplastic continuum. In order to assess the possibility of shear bifurcation in a general way, a condition for the peak stress state is provided. Geometric representations of the bifurcation states and peak stress states in the deviatoric stress plane are then presented, from which the accessibility of bifurcation points can be determined.

Symbolic notation is used for vectors and tensors in this paper. Vectors and second-order tensors are distinguished by bold-faced font and fourth-order tensors by calligraphic font. Index notation is used by referring to a fixed orthogonal Cartesian coordinate system. The second-order unit tensor and the fourth-order unit tensor are denoted by $\mathbf{I}$ and $\mathcal{I}$, respectively. Their components read $(\mathbf{I})_{ij} = \delta_{ij}$ and $(\mathcal{I})_{ijkl} = \delta_{ik}\delta_{jl}$ with δ_{ij} being the Kronecker delta. The permutation symbol $\boldsymbol{\epsilon}$ is used with $(\boldsymbol{\epsilon})_{ijk} = 1$ for $ijk \in \{\{1,2,3\},\{2,3,1\},\{3,1,2\}\}$, $(\boldsymbol{\epsilon})_{ijk} = -1$ for $ijk \in \{\{1,3,2\},\{2,1,3\},\{3,2,1\}\}$ and $(\boldsymbol{\epsilon})_{ijk} = 0$ otherwise. The dot-product operation is used for $\mathbf{a}\cdot\mathbf{b} = a_i b_i$, $(\mathbf{A}\cdot\mathbf{b})_i = A_{ij}b_j$, $\mathbf{A}:\mathbf{B} = A_{ij}B_{ij}$ and $(\mathcal{A}:\mathbf{B})_{ij} = A_{ijkl}B_{kl}$. Here, the usual summation convention for dummy indices is adopted. Dyadic multiplication is denoted by the symbol $\otimes$. For instance $(\mathbf{a}\otimes\mathbf{b})_{ij} = a_i b_j$ and $(\mathbf{A}\otimes\mathbf{B})_{ijkl} = A_{ij}B_{kl}$. The Euclidean norm is used for all vectors so that $\|\mathbf{a}\| = \sqrt{\mathbf{a}\cdot\mathbf{a}}$ and all tensors so that $\|\mathbf{A}\| = \sqrt{\mathbf{A}:\mathbf{A}}$. The Nabla operator $\boldsymbol{\nabla}$ is so defined that $(\boldsymbol{\nabla}\mathbf{a})_{ij} = \partial a_i/\partial x_j$ and $(\boldsymbol{\nabla}\cdot\mathbf{a}) = \partial a_i/\partial x_i$.

2. Hypoplastic description of granular materials

2.1. Outline of the micro-polar continuum

A micro-polar continuum is characterized by additional rotational degrees of freedom and the presence of a couple stress which is work-conjugated with the micro-curvature (associated with the rotational degrees of freedom). Material particles in a micro-polar continuum can translate and rotate independently. Here we use the vectors $\dot{\mathbf{u}}$ and $\dot{\mathbf{w}}^c$ to denote the rate of translation (velocity) and the rate of rotation (angular velocity) of material particles. Then the deformation rate of a micro-polar (Cosserat) continuum can be measured by the strain rate $\dot{\boldsymbol{\varepsilon}}^c$ and the micro-curvature rate $\dot{\boldsymbol{\kappa}}$, which are defined by the following kinematic relations:

$$\dot{\boldsymbol{\varepsilon}}^c = \nabla\dot{\mathbf{u}} + \boldsymbol{\epsilon}\cdot\dot{\mathbf{w}}^c, \quad \dot{\varepsilon}^c_{ij} = \partial\dot{u}_i/\partial x_j + \epsilon_{ijk}\dot{w}^c_k, \tag{1a}$$

$$\dot{\boldsymbol{\kappa}} = \nabla\dot{\mathbf{w}}^c, \qquad \dot{\kappa}_{ij} = \partial\dot{w}^c_i/\partial x_j. \tag{1b}$$

By introducing the notion of micro-spin $\dot{\boldsymbol{\omega}}^c = -\boldsymbol{\epsilon}\cdot\dot{\mathbf{w}}^c$, Equation (1a) can also be written in the form of:

$$\dot{\boldsymbol{\varepsilon}}^c = \dot{\boldsymbol{\varepsilon}} + \dot{\boldsymbol{\omega}} - \dot{\boldsymbol{\omega}}^c,$$

where $\dot{\boldsymbol{\varepsilon}} = \mathbf{d} = \frac{1}{2}[\nabla\dot{\mathbf{u}} + (\nabla\dot{\mathbf{u}})^T]$ and $\dot{\boldsymbol{\omega}} = \frac{1}{2}[\nabla\dot{\mathbf{u}} - (\nabla\dot{\mathbf{u}})^T]$, the symmetric part and the skew symmetric part of the velocity gradient, are the strain rate and the spin (termed the macro spin in this paper) for the non-polar continuum. The strain rate for the micro-polar continuum $\dot{\boldsymbol{\varepsilon}}^c$ is generally non-symmetric. In the case where the micro-spin coincides with the macro-spin, it becomes symmetric and coincides with the strain rate for the non-polar continuum.

The equilibrium equations for a micro-polar continuum must take into account the presence of the couple stress $\boldsymbol{\mu}$. In cases where body forces and body couples are absent, the *local* form of the equilibrium equations read:

$$\nabla\cdot\boldsymbol{\sigma}^T = \mathbf{0}, \qquad \partial\sigma_{ij}/\partial x_j = 0, \tag{2a}$$

$$\nabla\cdot\boldsymbol{\mu}^T - \boldsymbol{\epsilon}:\boldsymbol{\sigma} = \mathbf{0}, \quad \partial\mu_{ij}/\partial x_j - \epsilon_{ijk}\sigma_{jk} = 0. \tag{2b}$$

From the second equation, we see that the stress tensor is generally non-symmetric for a micro-polar continuum. When the couple stress vanishes, the stress tensor becomes symmetric.

2.2. Hypoplastic model for non-polar and micro-polar continuum

In hypoplasticity, the granular material is described as a continuum in terms of material state and material properties. The latter are represented by constitutive constants which do not change during loading. In a non-polar (conventional) continuum approach, the material state is characterized by the current stress $\boldsymbol{\sigma}$ and the void ratio e, while in a micro-polar continuum description the couple stress $\boldsymbol{\mu}$ is also included.

In the nonpolar continuum description, a practical hypoplastic constitutive equation for the cohesionless granular materials has the following general form [16]:

$$\mathring{\boldsymbol{\sigma}} = f_s(\mathcal{L}(\hat{\boldsymbol{\sigma}}):\dot{\boldsymbol{\varepsilon}} + f_{\mathrm{d}}\mathbf{N}(\hat{\boldsymbol{\sigma}})\|\dot{\boldsymbol{\varepsilon}}\|). \tag{3}$$

The objective time rate of the Cauchy stress, $\mathring{\boldsymbol{\sigma}}$, is a nonlinear function of the strain rate $\dot{\boldsymbol{\varepsilon}}$. Herein the fourth-order tensor $\mathcal{L}$ and the second-order tensor $\mathbf{N}$ are functions of the normalized stress $\hat{\boldsymbol{\sigma}} = \boldsymbol{\sigma}/\mathrm{tr}\ \boldsymbol{\sigma}$, and the scalar factors f_{s} and f_{d} (known as the stiffness factor and the density factor, respectively) are functions of the mean pressure $p = -\mathrm{tr}\ \boldsymbol{\sigma}/3$ and the void

ratio e. The elaborated nonlinear tensor-valued function allows the description of different stiffness for loading and unloading without employing the elastoplastic concept of decomposition of strain rate into an elastic part and a plastic part. As $\mathring{\boldsymbol{\sigma}}$ is a positively homogeneous of order one in $\dot{\boldsymbol{\varepsilon}}$, the rate-independent behavior is described by (3).

In a micropolar continuum extension [18] of constitutive equation (3), the objective time rate of the stress, $\mathring{\boldsymbol{\sigma}}$, and the objective time rate of couple stress, $\mathring{\boldsymbol{\mu}}$, are expressed as

$$\mathring{\boldsymbol{\sigma}} = f_{\mathrm{s}}[\mathcal{L}^{\sigma\sigma} : \dot{\boldsymbol{\varepsilon}}^{c} + \mathcal{L}^{\sigma\mu} : \dot{\boldsymbol{\kappa}}^{*} + f_{\mathrm{d}}\mathbf{N}^{\sigma} R], \tag{4a}$$

$$\mathring{\boldsymbol{\mu}} = d_{50} f_{\mathrm{s}}[\mathcal{L}^{\mu\mu} : \dot{\boldsymbol{\kappa}}^{*} + \mathcal{L}^{\mu\sigma} : \dot{\boldsymbol{\varepsilon}}^{c} + f_{\mathrm{d}}\mathbf{N}^{\mu} R], \tag{4b}$$

where d_{50} denotes the mean grain diameter, which is a natural length scale for granular materials, $\dot{\boldsymbol{\kappa}}^{*} = d_{50}\dot{\boldsymbol{\kappa}}$ is the scaled micro-curvature rate, and R is a combination of the norms of the strain rate and the micro-curvature rate in the form of

$$R = \sqrt{\dot{\boldsymbol{\varepsilon}} : \dot{\boldsymbol{\varepsilon}} + \delta^{2}\dot{\boldsymbol{\kappa}} : \dot{\boldsymbol{\kappa}}}, \tag{5}$$

where

$$\delta = (a_{\mu}/\hat{a}) d_{50} \tag{6}$$

is a characteristic length which scales the thickness of shear bands. The fourth-order tensors and the second-order tensors depend on the normalized stress tensor, $\hat{\boldsymbol{\sigma}}$, and the normalized couple-stress tensor, $\hat{\boldsymbol{\mu}} = \boldsymbol{\mu}/(d_{50}\mathrm{tr}\ \boldsymbol{\sigma})$, with the following representations:

$$\begin{aligned} &\mathcal{L}^{\sigma\sigma} = \hat{a}^{2}\mathcal{I} + \hat{\boldsymbol{\sigma}} \otimes \hat{\boldsymbol{\sigma}}, \quad \mathcal{L}^{\sigma\mu} = \hat{\boldsymbol{\sigma}} \otimes \hat{\boldsymbol{\mu}}, \quad \mathbf{N}^{\sigma} = \hat{a}(\hat{\boldsymbol{\sigma}} + \hat{\boldsymbol{\sigma}}^{d}), \\ &\mathcal{L}^{\mu\mu} = a_{\mu}^{2}\mathcal{I} + \hat{\boldsymbol{\mu}} \otimes \hat{\boldsymbol{\mu}}, \quad \mathcal{L}^{\mu\sigma} = \hat{\boldsymbol{\mu}} \otimes \hat{\boldsymbol{\sigma}}, \quad \mathbf{N}^{\mu} = 2\hat{a}\hat{\boldsymbol{\mu}}. \end{aligned} \tag{7}$$

Herein $\hat{\boldsymbol{\sigma}}^{d} = \hat{\boldsymbol{\sigma}} - \mathbf{I}/3$ denotes the deviator of the normalized stress, and $\hat{a}$ and a_{μ} are two parameters related to the limit value of stress and couple stress at stationary states.

A stationary state is reached when there is no change in the state variables under continuing deformation. The present micro-polar hypoplastic model is characterized by the following limit condition on the stress, the couple stress, and the void ratio at stationary states [18]:

$$\frac{\|\hat{\boldsymbol{\sigma}}^{d}\|^{2}}{\hat{a}^{2}} + \frac{\|\hat{\boldsymbol{\mu}}\|^{2}}{a_{\mu}^{2}} = 1 \quad \text{and} \quad f_{\mathrm{d}} = 1. \tag{8}$$

This relation shows a coupling between the limit stress and the limit couple stress. It also provides a physical interpretation for the parameters $\hat{a}$ and a_{μ}.

The evolution of the void ratio is governed by the equation:

$$\dot{e} = (1 + e)\mathrm{tr}\ \dot{\boldsymbol{\varepsilon}}, \tag{9}$$

which is a result of mass balance by neglecting the volume change in solid grains. The void ratio of a granular material is bounded by the maximum void ratio e_i for the loosest states and the minimum void ratio e_d for the densest state, and it tends to a critical void ratio e_c at stationary states. e_i, e_d and e_c are pressure-dependent quantities. In the present model, the variation of e_i, e_d and e_c with the mean pressure p is described by the following relation (refer to Figure 1):

$$\frac{e_c}{e_{co}} = \frac{e_d}{e_{do}} = \frac{e_i}{e_{io}} = \exp\{(3p/h_s)^{n}\}. \tag{10}$$

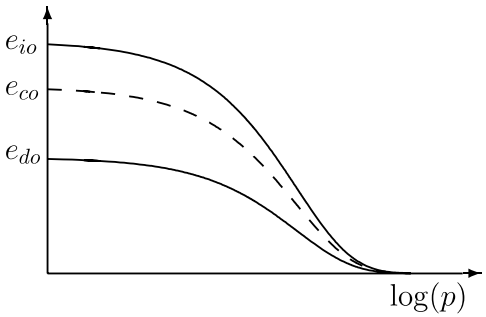

Figure 1. Pressure dependence of the maximum, the critic and the minimum void ratio [17].

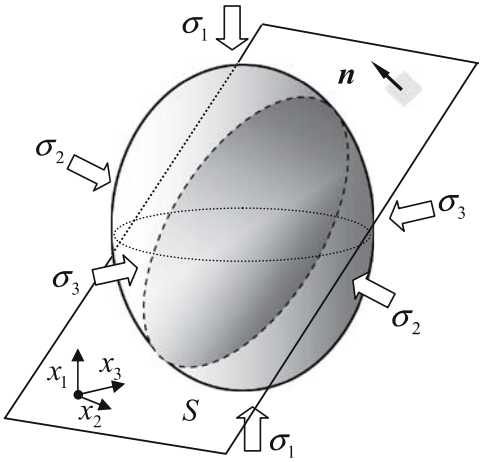

Figure 2. Sketch of weak discontinuity plane in the principal stress space.

Herein h_s and n are two material constants that determine the shape of the void ratio-pressure curves, and e_{io}, e_{do} and e_{co} are three material constants which represent the maximum, minimum and critical void ratio at the stress-free state. The density factor f_d is related to the pressure-dependent relative density according to

$$f_\mathrm{d} = \left(\frac{e - e_d}{e_c - e_d}\right)^{\alpha}, \tag{11}$$

where α is a material constant which scales the peak stress state under loading. Note that dilative deformation corresponds to an increase in the value for f_d. The densest state is characterized by $f_\mathrm{d} = 0$, while $f_\mathrm{d} = 1$ corresponds to $e = e_c$. Therefore, the critical void ratio is reached at a stationary state, which is in accordance with experimental observations for granular materials.

The stiffness factor f_s has the following representation:

$$f_\mathrm{s} = \frac{h_s}{n(\hat{\boldsymbol{\sigma}} : \hat{\boldsymbol{\sigma}})} \left(\frac{e_i}{e}\right)^{\beta} \frac{1 + e_i}{e_i} \left(\frac{p}{h_s}\right)^{(1-n)} [3\hat{a}_i^2 + 1 + \sqrt{3}\hat{a}_i f_{di}]^{-1}. \tag{12}$$

Herein f_{di} and a_i represent the values of f_d and $\hat{a}$ at isotropic states. From (10) and (11), f_{di} has a constant value $f_{di} = \{(e_{io} - e_{do})/(e_{co} - e_{do})\}^{\alpha}$. As described later, a_i has a constant value, which is related to the critical friction angle ϕ_c. The term $(e_i/e)^{\beta}$ reflects the influence of the density on the stiffness factor with $\beta \approx 1$ being another material constant.

For the special case where the couple stress and micro-curvature rate vanish and the micro-spin coincides with the macro-spin, the non-polar continuum model proposed by Gudehus [16] and Bauer [17] is recovered with

$$\mathcal{L}^{\sigma\sigma} = \mathcal{L} = \hat{a}^2 \mathcal{I} + \hat{\boldsymbol{\sigma}} \otimes \hat{\boldsymbol{\sigma}}, \quad \mathbf{N}^{\sigma} = \mathbf{N} = \hat{a}(\hat{\boldsymbol{\sigma}} + \hat{\boldsymbol{\sigma}}^d). \tag{13}$$

Correspondingly, the limit stress at a stationary state satisfies the following condition:

$$||\hat{\boldsymbol{\sigma}}^d|| = \hat{a}, \tag{14}$$

which represents a conical surface in the principal stress space with its apex at the origin. Bauer [28] showed that it is possible to embed different limit stress conditions into this model

by adopting different expressions for the parameter $\hat{a}$. For instance, a constant value for $\hat{a}$ corresponds to a Drucker–Prage type limit condition. With the following formulation, the Matsuoka–Nakai limit condition is embedded:

$$\hat{a} = \frac{\sin\varphi_c}{3-\sin\varphi_c}\left[\sqrt{\frac{8/3-3||\hat{\boldsymbol{\sigma}}^{sd}||^2+\sqrt{3/2}||\hat{\boldsymbol{\sigma}}^{sd}||^3\cos(3\theta)}{1+\sqrt{3/2}||\hat{\boldsymbol{\sigma}}^{sd}||\cos(3\theta)}}-||\hat{\boldsymbol{\sigma}}^{sd}||\right], \tag{15}$$

where $\hat{\boldsymbol{\sigma}}^{sd}$ denotes the deviator of the normalized symmetric stress, and θ denotes the Lode angle defined in the deviatoric stress plane for the symmetric stress.

The limit couple stress related parameter a_μ is considered to be constant. For a granular material without preferred grain orientation, this is a reasonable assumption. All the material constants in this model, except a_μ, can be determined easily from elementary laboratory tests as discussed in detail by Herle and Gudehus [29]. a_μ may be determined from a back analysis procedure after measuring the shear band thickness, which requires advanced techniques. For the following discussion we note that the stiffness factor f_s has a value of the order of $h_s^n p^{1-n}$. The granular hardness (as termed in Gudehus [16]) h_s, which has a dimension of stress, has a typical value of the order of $1{\cdot}0\times10^6$ kPa or higher for sands. The dimensionless exponent n falls in the range of $(0{\cdot}25, 0{\cdot}5)$ [29].

3. Bifurcation analysis for the non-polar hypoplastic continuum

Consider a homogeneous specimen under uniform deformation and assume that the velocity and stress fields are continuous up to a certain state where a discontinuity in the velocity gradient across a planar surface becomes possible. This weak discontinuity plane S is then characterized by the following kinematic conditions:

$$[[\mathbf{l}]] = [[\nabla\dot{\mathbf{u}}]] = (\nabla\dot{\mathbf{u}})^1 - (\nabla\dot{\mathbf{u}})^0 = \mathbf{g}\otimes\mathbf{n} \quad \text{and} \quad [[\dot{\mathbf{u}}]] = \dot{\mathbf{u}}^1 - \dot{\mathbf{u}}^0 = 0. \tag{16}$$

Here the superscript 0 and 1 are used to denote the values for a quantity on either side of the discontinuity plane. Equation (16) states that across the discontinuous plane S the velocity gradient is experiencing a jump, which is characterized by a vector $\mathbf{g}$ and the unit normal vector $\mathbf{n}$ to the discontinuity plane, while the velocity field itself is continuous. Corresponding to the discontinuous velocity gradient, jumps in the strain rate and the spin tensor will be encountered on crossing S:

$$[[\dot{\boldsymbol{\varepsilon}}]] = \dot{\boldsymbol{\varepsilon}}^1 - \dot{\boldsymbol{\varepsilon}}^0 = \frac{1}{2}(\mathbf{g}\otimes\mathbf{n}+\mathbf{n}\otimes\mathbf{n}), \tag{17a}$$

$$[[\dot{\boldsymbol{\omega}}]] = \dot{\boldsymbol{\omega}}^1 - \dot{\boldsymbol{\omega}}^0 = \frac{1}{2}(\mathbf{g}\otimes\mathbf{n}-\mathbf{n}\otimes\mathbf{g}). \tag{17b}$$

In response to this, the stress rate becomes discontinuous. A bifurcation condition can be formulated by considering rate-form equilibrium long the possible discontinuity plane. Concerning the fact that the direction of the discontinuity plane varies with time due to the motion, we start to consider the equilibrium in a reference configuration (A reference configuration is a fixed configuration in the space which uniquely designates a one-to-one mapping with material points in motion.). On the image discontinuity plane in the reference configuration, the nominal traction rate must be unique, *i.e.*, $[[\dot{\mathbf{P}}]]\cdot\mathbf{N}=\mathbf{0}$, where $\mathbf{P}$ is the first Piola–Kirchhoff stress and $\mathbf{N}$ is the unit normal of the image discontinuity plane, which is independent of time. Using the well-known relation $\mathbf{P} = J\boldsymbol{\sigma}\cdot\mathbf{F}^{-T}$ and the Nanson's formula (see, for instance, [30,

p. 75]) the following equation is obtained:

$$[[\dot{\boldsymbol{\sigma}} + (\operatorname{div}\dot{\mathbf{u}})\boldsymbol{\sigma} - \boldsymbol{\sigma}\cdot\mathbf{l}^T]]\cdot\mathbf{n} = [[\dot{\boldsymbol{\sigma}}]]\cdot\mathbf{n} + ([[\operatorname{div}\dot{\mathbf{u}}]]\boldsymbol{\sigma} - \boldsymbol{\sigma}\cdot[[\mathbf{l}^T]])\cdot\mathbf{n} = 0. \tag{18}$$

Note that the material response is described in terms of the objective time rates of stress and couple stress. There is an infinite number of possibilities which define an objective time rate for the stress tensor. The most widely used objective stress rates include the Zaremba–Jaumann rate, the Oldroyd rate, the Green–Naghdi rate and the Truesdell rate ([30, Section5.3]). Choosing a proper objective stress rate is, in many cases, a problem of a proper formulation of the constitutive equations. It should also be noted that the discrepancies due to the choice of different objective stress rates become significant only when a large shear deformation has taken place (*e.g.* [28]). At the beginning of shear localization, such discrepancies are negligible. In this study, we take the Zaremba–Jaumann rate as the objective time rate for both the stress tensor and the couple stress tensor:

$$\mathring{\boldsymbol{\sigma}} = \dot{\boldsymbol{\sigma}} - (\dot{\boldsymbol{\omega}}\cdot\boldsymbol{\sigma} - \boldsymbol{\sigma}\cdot\dot{\boldsymbol{\omega}}), \tag{19a}$$

$$\mathring{\boldsymbol{\mu}} = \dot{\boldsymbol{\mu}} - (\dot{\boldsymbol{\omega}}\cdot\boldsymbol{\mu} - \boldsymbol{\mu}\cdot\dot{\boldsymbol{\omega}}). \tag{19b}$$

Substitution of (19a) in (18) yields the following bifurcation condition

$$[[\mathring{\boldsymbol{\sigma}}]]\cdot\mathbf{n} + ([[\operatorname{div}\dot{\mathbf{u}}]]\boldsymbol{\sigma}\cdot\mathbf{n} + [[\dot{\boldsymbol{\omega}}]]\cdot\boldsymbol{\sigma}\cdot\mathbf{n} - \boldsymbol{\sigma}\cdot[[\mathbf{d}]])\cdot\mathbf{n} = 0. \tag{20}$$

Invoking the constitutive relations leads to the following equations for the components of the vector $\mathbf{g}$:

$$\mathbf{K}\cdot\mathbf{g} - \lambda f_{\mathrm{d}}\mathbf{r} = 0. \tag{21}$$

The following notations are introduced in this equation: the scalar factor $\lambda = ||\dot{\boldsymbol{\varepsilon}}^1|| - ||\dot{\boldsymbol{\varepsilon}}^0||$, the vector $\mathbf{r} = -\hat{a}(\hat{\boldsymbol{\sigma}} + \hat{\boldsymbol{\sigma}}^d)\cdot\mathbf{n}$ and the tensor $\mathbf{K} = \mathbf{K}' + \mathbf{K}''$, where

$$\begin{aligned}\mathbf{K}' &= \tfrac{\hat{a}^2}{2}(\mathbf{I} + \mathbf{n}\otimes\mathbf{n}) + (\hat{\boldsymbol{\sigma}}\cdot\mathbf{n})\otimes(\hat{\boldsymbol{\sigma}}\cdot\mathbf{n}),\\ \mathbf{K}'' &= -\tfrac{3p}{f_{\mathrm{s}}}[\hat{\boldsymbol{\sigma}}\cdot\mathbf{n}\otimes\mathbf{n} - \mathbf{n}\otimes\mathbf{n}\cdot\hat{\boldsymbol{\sigma}}^T].\end{aligned} \tag{22}$$

In the representation for $\mathbf{K}''$, the factor $-3p$ comes out from the stress normalization. Since the stiffness factor $f_{\mathrm{s}} \sim h_s^n p^{1-n}$, it follows that the factor p/f_{s} has a value of the order of $(p/h_s)^n$. Therefore, for most practical stress states with $p << h_s$, $\mathbf{K}'$ is the dominant term in $\mathbf{K}$ and $\mathbf{K}''$ can be neglected. Because $\mathbf{K}'$ is positive-definite and therefore invertible, $\mathbf{K}$ is also invertible. Then we can write $\mathbf{g}$ as a linear function of the scalar factor λ:

$$\mathbf{g} = \lambda f_{\mathrm{d}}\mathbf{K}^{-1}\cdot\mathbf{r}. \tag{23}$$

For $\lambda = 0$, we have only a null solution for $\mathbf{g}$, which indicates no bifurcation at all. Thus the bifurcation problem is equivalent to seeking a non-trivial solution for the scalar factor λ. By introducing the notations

$$\hat{\mathbf{g}} = \mathbf{K}^{-1}\cdot\mathbf{r} \quad \text{and} \quad \Delta\hat{\boldsymbol{\varepsilon}} = \frac{1}{2}(\hat{\mathbf{g}}\otimes\mathbf{n} + \mathbf{n}\otimes\hat{\mathbf{g}}), \tag{24}$$

we can write the strain rate as $\dot{\boldsymbol{\varepsilon}}^1 = \dot{\boldsymbol{\varepsilon}}^0 + \lambda f_{\mathrm{d}}\Delta\hat{\boldsymbol{\varepsilon}}$. It follows that the nonlinear equation for the scalar factor λ can be written as

$$\lambda - \left(\sqrt{(\dot{\boldsymbol{\varepsilon}}^0 + \lambda f_{\mathrm{d}}\Delta\boldsymbol{\varepsilon}) : (\dot{\boldsymbol{\varepsilon}}^0 + \lambda f_{\mathrm{d}}\Delta\boldsymbol{\varepsilon})} - \sqrt{\dot{\boldsymbol{\varepsilon}}^0 : \dot{\boldsymbol{\varepsilon}}^0}\right) = 0. \tag{25}$$

Algebraic manipulation leads to the following equation:

$$(f_d^2 \Delta\hat{\boldsymbol{\varepsilon}} : \Delta\hat{\boldsymbol{\varepsilon}} - 1))\lambda^2 + 2(f_d \dot{\boldsymbol{\varepsilon}}^0 : \Delta\hat{\boldsymbol{\varepsilon}} - \|\dot{\boldsymbol{\varepsilon}}^0\|)\lambda = 0.$$

The non-trivial solution for λ then reads

$$\lambda = 2\frac{\|\dot{\boldsymbol{\varepsilon}}^0\| - f_d \dot{\boldsymbol{\varepsilon}}^0 : \Delta\hat{\boldsymbol{\varepsilon}}}{f_d^2 \Delta\hat{\boldsymbol{\varepsilon}} : \Delta\hat{\boldsymbol{\varepsilon}} - 1} = 2\frac{1 - f_d \|\Delta\hat{\boldsymbol{\varepsilon}}\| \cos\gamma}{f_d^2 \Delta\hat{\boldsymbol{\varepsilon}} : \Delta\hat{\boldsymbol{\varepsilon}} - 1}\|\dot{\boldsymbol{\varepsilon}}^0\| \tag{26}$$

with $\cos\gamma := (\dot{\boldsymbol{\varepsilon}}^0 : \Delta\hat{\boldsymbol{\varepsilon}})/(\|\dot{\boldsymbol{\varepsilon}}^0\|\|\Delta\hat{\boldsymbol{\varepsilon}}\|)$. Note that λ is restricted by the condition

$$\lambda \geq -\|\dot{\boldsymbol{\varepsilon}}^0\|, \tag{27}$$

since $\|\dot{\boldsymbol{\varepsilon}}\| = \lambda + \|\dot{\boldsymbol{\varepsilon}}^0\| \geq 0$. It can be shown that the requirement (27) can be fulfilled only when

$$f_d^2 \Delta\hat{\boldsymbol{\varepsilon}} : \Delta\hat{\boldsymbol{\varepsilon}} = \frac{f_d^2}{2}[\hat{\mathbf{g}} \cdot \hat{\mathbf{g}} + (\hat{\mathbf{g}} \cdot \mathbf{n})^2] \geq 1. \tag{28}$$

Proof. Assume that (28) is not fulfilled, then $f_d\|\Delta\hat{\boldsymbol{\varepsilon}}\| < 1$. The maximum value for λ in (26) corresponds to $\cos\gamma = 1$, which reads

$$\lambda_{\max} = -\frac{2}{1 + f_d\|\Delta\hat{\boldsymbol{\varepsilon}}\|}\|\dot{\boldsymbol{\varepsilon}}^0\| < -\|\dot{\boldsymbol{\varepsilon}}^0\|, \tag{29}$$

which violates the requirement (27).

Remark. Inequality (28) can also be obtained in an alternative way. Note that a triangular inequality $\|\dot{\boldsymbol{\varepsilon}}^1 - \dot{\boldsymbol{\varepsilon}}^0\|^2 \geq (\|\dot{\boldsymbol{\varepsilon}}^1\| - \|\dot{\boldsymbol{\varepsilon}}^0\|)^2$ is generally valid. Substitution of $(\|\dot{\boldsymbol{\varepsilon}}^1\| - \|\dot{\boldsymbol{\varepsilon}}^0\|)^2 = \lambda^2$ and $\|\dot{\boldsymbol{\varepsilon}}^1 - \dot{\boldsymbol{\varepsilon}}^0\|^2 = \lambda^2 f_d^2(\hat{\mathbf{g}} \cdot \hat{\mathbf{g}} + (\hat{\mathbf{g}} \cdot \mathbf{n})^2)/2$ leads to inequality (28). This approach is simpler. However, the approach from (25) to (28) provides more detail about the factor λ and can be repeated for derivation of the bifurcation criterion for the micro-polar continuum model.

Remark. The equality in (28) corresponds to either $||\dot{\boldsymbol{\varepsilon}}^1||/||\dot{\boldsymbol{\varepsilon}}^0|| = \infty$ or $\cos\gamma = 1$. The later is true only when $\dot{\boldsymbol{\varepsilon}}^1$ is co-axial with $\dot{\boldsymbol{\varepsilon}}^0$, which corresponds to pure dilation or contraction in the localized zone. For a uniformly deforming process leading to a continuous onset of shear bifurcation, the equality represents a limit state at which the bifurcation will not occur.

To assess whether the bifurcation condition is met in a loading program, the equality can be used as a determinant. That is, incipience of shear localization is indicated by the following condition:

$$f_d^2 \Phi_0(\hat{\boldsymbol{\sigma}}, \mathbf{n}) - 1 = 0, \tag{30}$$

with

$$\Phi_0(\hat{\boldsymbol{\sigma}}, \mathbf{n}) = \frac{1}{2}[\hat{\mathbf{g}} \cdot \hat{\mathbf{g}} + (\hat{\mathbf{g}} \cdot \mathbf{n})^2] = \frac{1}{2}[(\mathbf{K}^{-1} \cdot \mathbf{r}) \cdot (\mathbf{K}^{-1} \cdot \mathbf{r}) + (\mathbf{n} \cdot \mathbf{K}^{-1} \cdot \mathbf{r})^2]. \tag{31}$$

Note that for $p << h_s$, $\mathbf{K}''$ can be neglected in the representation of $\mathbf{K}$. In the case where $p \sim h_s$ or $p > h_s$, we have $e_i/e \sim 1$, which implies that f_s and $\mathbf{K}''$ are almost independent of the void ratio. Therefore, in the criterion (30), Φ_0 can be considered independent of the density. The influence of the density on bifurcation is reflected only by the factor f_d, which is separated from Φ_0.

4. Bifurcation analysis for the micro-polar hypoplastic continuum

Similar conditions for weak-discontinuity bifurcation can be formulated for a micro-polar hypoplastic continuum. We start again with a homogeneously deforming specimen in which the velocity, rotation rate, stress and couple stress fields are continuous up to a state where a banded planar weak discontinuity may develop. Across the weak discontinuity plane S, the velocity and the rotation rate fields are initially continuous:

$$[[\dot{\mathbf{u}}]] = \dot{\mathbf{u}}^1 - \dot{\mathbf{u}}^0 = 0 \quad \text{and} \quad [[\dot{\mathbf{w}}^c]] = \dot{\mathbf{w}}^{c1} - \dot{\mathbf{w}}^{c0} = 0\,, \tag{32}$$

while the jump in the velocity gradient and the rotation-rate gradient can be written as

$$[[\nabla\dot{\mathbf{u}}]] = (\nabla\dot{\mathbf{u}})^1 - (\nabla\dot{\mathbf{u}})^0 = \mathbf{g}^u \otimes \mathbf{n}, \tag{33a}$$

$$[[\dot{\boldsymbol{\kappa}}]] = (\nabla\dot{\mathbf{w}}^c)^1 - (\nabla\dot{\mathbf{w}}^c)^0 = \mathbf{g}^w \otimes \mathbf{n}. \tag{33b}$$

Weak discontinuity bifurcation is characterized by vectors $\mathbf{g}^u, \mathbf{g}^w$ and the unit normal vector $\mathbf{n}$ for the discontinuity plane S. With respect to the discontinuity in the velocity gradient, the jumps in the strain rate and in the macro-spin read

$$[[\dot{\boldsymbol{\varepsilon}}^c]] = \dot{\boldsymbol{\varepsilon}}^{c1} - \dot{\boldsymbol{\varepsilon}}^{c0} = [[\nabla\dot{\mathbf{u}} + \boldsymbol{\epsilon}\cdot\mathbf{w}^c]] = \mathbf{g}^u \otimes \mathbf{n}, \tag{34a}$$

$$[[\dot{\boldsymbol{\omega}}]] = \dot{\boldsymbol{\omega}}^1 - \dot{\boldsymbol{\omega}}^0 = \frac{1}{2}(\mathbf{g}^u \otimes \mathbf{n} - \mathbf{n} \otimes \mathbf{g}^u). \tag{34b}$$

Similar to the situation for the nonpolar continuum, consideration of the equilibrium in rate form along the discontinuity plane leads to the following conditions to be fulfilled by the total stress rate and the total couple stress rate:

$$[[\dot{\boldsymbol{\sigma}}]]\cdot\mathbf{n} + ([[\operatorname{div}\dot{\mathbf{u}}]]\boldsymbol{\sigma} - \boldsymbol{\sigma}\cdot[[\mathbf{I}^T]])\cdot\mathbf{n} = 0, \tag{35a}$$

$$[[\dot{\boldsymbol{\mu}}]]\cdot\mathbf{n} + ([[\operatorname{div}\dot{\mathbf{u}}]]\boldsymbol{\mu} - \boldsymbol{\mu}\cdot[[\mathbf{I}^T]])\cdot\mathbf{n} = 0. \tag{35b}$$

Using the expressions for stress rate (19a) and couple-stress rate (19b) and the constitutive Equations (4a) and (4b), the following nonlinear equations are obtained for the vectors $\mathbf{g}^u$ and $\mathbf{g}^w$:

$$\mathbf{K}_{uu}\cdot\mathbf{g}^u + \mathbf{K}_{uw}\cdot\mathbf{g}^w - \lambda^c f_{\mathrm{d}}\mathbf{r}^u = 0, \tag{36a}$$

$$\mathbf{K}_{wu}\cdot\mathbf{g}^u + \mathbf{K}_{ww}\cdot\mathbf{g}^w - \lambda^c f_{\mathrm{d}}\mathbf{r}^w = 0. \tag{36b}$$

Herein the following notations are used: the scalar factor $\lambda^c = [[R]]$, the vectors $\mathbf{r}^u = -\hat{a}(\hat{\boldsymbol{\sigma}} + \hat{\boldsymbol{\sigma}}^d)\cdot\mathbf{n}$ and $\mathbf{r}^w = -2\hat{a}\hat{\boldsymbol{\mu}}\cdot\mathbf{n}$, and the tensors $\mathbf{K}_{uu} = \mathbf{K}'_{uu} + \mathbf{K}''_{uu}$, $\mathbf{K}_{uw} = \mathbf{K}'_{uw}$, $\mathbf{K}_{wu} = \mathbf{K}'_{wu} + \mathbf{K}''_{wu}$ and $\mathbf{K}_{ww} = \mathbf{K}'_{ww}$ with the following representations:

$$\begin{aligned}
\mathbf{K}'_{uu} &= \hat{a}^2\mathbf{I} + (\hat{\boldsymbol{\sigma}}\cdot\mathbf{n})\otimes(\hat{\boldsymbol{\sigma}}\cdot\mathbf{n}), \quad \mathbf{K}'_{uw} = d_{50}(\hat{\boldsymbol{\sigma}}\cdot\mathbf{n})\otimes(\hat{\boldsymbol{\mu}}\cdot\mathbf{n}),\\
\mathbf{K}'_{wu} &= (\hat{\boldsymbol{\mu}}\cdot\mathbf{n})\otimes(\hat{\boldsymbol{\sigma}}\cdot\mathbf{n}), \quad \mathbf{K}'_{ww} = d_{50}[a_\mu^2\mathbf{I} + (\hat{\boldsymbol{\mu}}\cdot\mathbf{n})\otimes(\hat{\boldsymbol{\mu}}\cdot\mathbf{n})],\\
\mathbf{K}''_{uu} &= -\tfrac{3p}{f_s}[\hat{\boldsymbol{\sigma}}\cdot\mathbf{n}\otimes\mathbf{n} - \mathbf{n}\otimes\mathbf{n}\cdot\hat{\boldsymbol{\sigma}}^T],\\
\mathbf{K}''_{wu} &= -\tfrac{3p}{f_s}[\hat{\boldsymbol{\mu}}\cdot\mathbf{n}\otimes\mathbf{n} - \mathbf{n}\otimes\mathbf{n}\cdot\hat{\boldsymbol{\mu}}^T].
\end{aligned} \tag{37}$$

For a concise representation, we define $\boldsymbol{\Pi}$ according to

$$\boldsymbol{\Pi} := \begin{bmatrix} \mathbf{K}_{uu} & \mathbf{K}_{uw} \\ \mathbf{K}_{wu} & \mathbf{K}_{ww} \end{bmatrix}. \tag{38}$$

By neglecting $\mathbf{K}''_{uu}$ and $\mathbf{K}''_{wu}$ in $\mathbf{K}_{uu}$ and $\mathbf{K}_{wu}$ for $p << h_s$, we can show that $\mathbf{\Pi}$ is invertible (see appendix A). We can then write

$$\begin{Bmatrix} \mathbf{g}^u \\ \mathbf{g}^w \end{Bmatrix} = \lambda^c f_{\mathrm{d}} \mathbf{\Pi}^{-1} \cdot \begin{Bmatrix} \mathbf{r}^u \\ \mathbf{r}^w \end{Bmatrix}. \tag{39}$$

Again the bifurcation vectors $\mathbf{g}^u$ and $\mathbf{g}^w$ are linearly related to the scalar factor λ^c. Thus the problem is equivalent to seeking a non-trivial solution for the scalar factor λ^c. By introducing the following notations

$$\begin{Bmatrix} \hat{\mathbf{g}}^u \\ \hat{\mathbf{g}}^w \end{Bmatrix} = \mathbf{\Pi}^{-1} \cdot \begin{Bmatrix} \mathbf{r}^u \\ \mathbf{r}^w \end{Bmatrix} \tag{40}$$

and

$$\Delta\hat{\boldsymbol{\varepsilon}}^c = \hat{\mathbf{g}}^u \otimes \mathbf{n}, \quad \Delta\hat{\boldsymbol{\kappa}} = \hat{\mathbf{g}}^w \otimes \mathbf{n}, \tag{41}$$

the equation for the factor λ^c can be written as

$$\begin{aligned} &\lambda^c + \sqrt{\dot{\boldsymbol{\varepsilon}}^{c0} : \dot{\boldsymbol{\varepsilon}}^{c0} + \delta^2 \dot{\boldsymbol{\kappa}}^0 : \delta^2 \dot{\boldsymbol{\kappa}}^0} \\ &\quad = \sqrt{(\dot{\boldsymbol{\varepsilon}}^{c0} + \lambda^c f_{\mathrm{d}} \Delta\hat{\boldsymbol{\varepsilon}}^c) : (\dot{\boldsymbol{\varepsilon}}^{c0} + \lambda^c f_{\mathrm{d}} \Delta\hat{\boldsymbol{\varepsilon}}^c) + \delta^2 (\dot{\boldsymbol{\kappa}}^0 + \lambda^c f_{\mathrm{d}} \Delta\hat{\boldsymbol{\kappa}}) : (\dot{\boldsymbol{\kappa}}^0 + \lambda^c f_{\mathrm{d}} \Delta\hat{\boldsymbol{\kappa}})}. \end{aligned} \tag{42}$$

The non-trivial solution for λ^c reads

$$\lambda^c = 2 \frac{1 - f_{\mathrm{d}} (\dot{\boldsymbol{\varepsilon}}^{c0} : \Delta\hat{\boldsymbol{\varepsilon}}^c + \delta^2 \dot{\boldsymbol{\kappa}}^0 : \Delta\boldsymbol{\kappa}) / \sqrt{\|\dot{\boldsymbol{\varepsilon}}^{c0}\|^2 + \delta^2 \|\dot{\boldsymbol{\kappa}}^0\|^2}}{f_{\mathrm{d}}^2 (\|\Delta\hat{\boldsymbol{\varepsilon}}^c\|^2 + \delta^2 \|\Delta\hat{\boldsymbol{\kappa}}\|^2) - 1} \times \sqrt{\|\dot{\boldsymbol{\varepsilon}}^{c0}\|^2 + \delta^2 \|\dot{\boldsymbol{\kappa}}^0\|^2}. \tag{43}$$

Here λ^c is restricted by a requirement similar to (27), which reads

$$\lambda^c \geq -\sqrt{\|\dot{\boldsymbol{\varepsilon}}^{c0}\|^2 + \delta^2 \|\dot{\boldsymbol{\kappa}}^0\|^2}. \tag{44}$$

In a similar way, we can show that this requirement can be fulfilled only when

$$f_{\mathrm{d}}^2 (\|\Delta\hat{\boldsymbol{\varepsilon}}^c\|^2 + \delta^2 \|\Delta\boldsymbol{\kappa}\|^2) \geq 1. \tag{45}$$

Proof. Since $\dot{\boldsymbol{\varepsilon}}^{c0} : \Delta\hat{\boldsymbol{\varepsilon}}^c \leq \|\dot{\boldsymbol{\varepsilon}}^{c0}\| \|\Delta\hat{\boldsymbol{\varepsilon}}^c\|$ and $\dot{\boldsymbol{\kappa}}^0 : \Delta\hat{\boldsymbol{\kappa}} \leq \|\dot{\boldsymbol{\kappa}}^0\| \|\Delta\hat{\boldsymbol{\kappa}}\|$, we have

$$(\dot{\boldsymbol{\varepsilon}}^{c0} : \Delta\hat{\boldsymbol{\varepsilon}}^c + \delta^2 \dot{\boldsymbol{\kappa}}^0 : \Delta\boldsymbol{\kappa})^2 \leq (\|\dot{\boldsymbol{\varepsilon}}^{c0}\|^2 + \delta^2 \|\dot{\boldsymbol{\kappa}}^0\|^2)(\|\Delta\hat{\boldsymbol{\varepsilon}}^c\|^2 + \delta^2 \|\Delta\boldsymbol{\kappa}\|^2).$$

If follows that the following inequality is valid.

$$f_{\mathrm{d}} (\dot{\boldsymbol{\varepsilon}}^{c0} : \Delta\hat{\boldsymbol{\varepsilon}}^c + \delta^2 \dot{\boldsymbol{\kappa}}^0 : \Delta\boldsymbol{\kappa}) / \sqrt{\|\dot{\boldsymbol{\varepsilon}}^{c0}\|^2 + \delta^2 \|\dot{\boldsymbol{\kappa}}^0\|^2} \leq f_{\mathrm{d}} \sqrt{\|\Delta\hat{\boldsymbol{\varepsilon}}^c\|^2 + \delta^2 \|\Delta\boldsymbol{\kappa}\|^2}.$$

Assume that (45) is not fulfilled, then $f_{\mathrm{d}} \sqrt{\|\Delta\hat{\boldsymbol{\varepsilon}}^c\|^2 + \delta^2 \|\Delta\boldsymbol{\kappa}\|^2} < 1$. The maximum value for λ^c in (43) can be obtained as

$$\lambda^c_{\max} = -\frac{2}{1 + f_{\mathrm{d}} \sqrt{\|\Delta\hat{\boldsymbol{\varepsilon}}^c\|^2 + \delta^2 \|\Delta\boldsymbol{\kappa}\|^2}} \sqrt{\|\dot{\boldsymbol{\varepsilon}}^{c0}\|^2 + \delta^2 \|\dot{\boldsymbol{\kappa}}^0\|^2} < -\sqrt{\|\dot{\boldsymbol{\varepsilon}}^{c0}\|^2 + \delta^2 \|\dot{\boldsymbol{\kappa}}^0\|^2},$$

which violates the requirement (44). Therefore, the occurrence of shear bifurcation in the micro-polar hypoplastic continuum can be judged by the following criterion:

$$f_{\mathrm{d}}^2 \Phi_1 (\hat{\boldsymbol{\sigma}}, \hat{\boldsymbol{\mu}}, \mathbf{n}) - 1 = 0, \tag{46}$$

where

$$\Phi_1(\hat{\boldsymbol{\sigma}}, \hat{\boldsymbol{\mu}}, \mathbf{n}) = (\|\Delta\hat{\boldsymbol{\varepsilon}}^c\|^2 + \delta^2\|\Delta\boldsymbol{\kappa}\|^2) = \hat{\mathbf{g}}^u \cdot \hat{\mathbf{g}}^u + \delta^2\hat{\mathbf{g}}^w \cdot \hat{\mathbf{g}}^w. \tag{47}$$

It has been widely recognized that polar effects are usually associated with pronounced strain gradients. A homogeneous specimen under uniform deformation is almost always free from polar effects, that is, the couple stress and the micro-curvature will not develop up to a shear bifurcation state. Therefore we have $\boldsymbol{\mu} = \mathbf{0}$ at the incipience of bifurcation, and the bifurcation condition (36b) is reduced to yield $\mathbf{g}^w = \mathbf{0}$. Thus the bifurcation criterion (46) for the micro-polar hypoplastic continuum is simplified to

$$f_d^2\Phi_1^*(\hat{\boldsymbol{\sigma}}, \mathbf{n}) - 1 = 0 \tag{48}$$

and

$$\Phi_1^*(\hat{\boldsymbol{\sigma}}, \mathbf{n}) = \hat{\mathbf{g}}^u \cdot \hat{\mathbf{g}}^u = (\mathbf{K}_{uu}^{-1} \cdot \mathbf{r}^u) \cdot (\mathbf{K}_{uu}^{-1} \cdot \mathbf{r}^u). \tag{49}$$

5. Examination of bifurcation condition

Granular materials show strong pressure- and density-sensitive behavior. For an initially dense specimen under monotonic loading to a stationary state, the deviatoric stress will show a peak with the specimen experiencing dilation after an initial contraction. The denser the specimen is packed, the higher the peak and the stronger the dilation will be. The peak will be less pronounced at a higher pressure level. If a specimen is initially in a very loose state, no peak state will be displayed and the specimen will experience a consistent contraction without dilation. This pressure and density effect has been taken into account in the present hypoplastic model by including the void ratio as a state variable. For monotonic loading paths, accessible stress states are bounded by the peak stress states, which form a conical surface in the principal stress space with its apex at the origin and its axis aligned with the hydro-static pressure axis.

With regard to criteria (30) and (46), we note that shear bifurcation depends on the stress and density for a non-polar continuum and the stress, couple stress and density for a micro-polar continuum (the couple stress often equals zero in a homogeneously deforming specimen). Shear bifurcation will occur in a homogeneously deforming specimen as the criterion (30) or (46) is met by the varying stress and density. For the non-polar continuum model, it has been shown that shear bifurcation occurs before the peak stress state is reached in biaxial compression tests [23, 24]. The bifurcation point and the inclination of the shear band are influenced by the initial density and the mean pressure. Wu and Sikora [25] and Wu [26], in their analysis for bifurcation and failure in a density-independent non-polar hypoplastic continuum, have shown that the peak stress state may be reached before the bifurcation condition is met for some loading paths. This means a homogeneously deforming specimen may experience either a homogeneous failure or a localized failure, depending on the loading path.

In order to investigate the possibility of bifurcation in a general way for the present continuum models, we will compare the bifurcation states with the peak stress states in the deviatoric stress plane, as done by Wu [26] for a density-independent hypoplastic model. For this purpose, a mathematical representation for the peak stress state is formulated in the following.

5.1. Peak stress state

A peak stress state is defined by a vanishing stress rate with $\dot{e} > 0$. Note that a peak state differs from a stationary state in that the void ratio vanishes simultaneously with the latter. We consider loading programs such that the directions of the principal stresses do not change while the deviatoric stress varies. Triaxial compression and extension, as well as biaxial compression and extension tests, are examples of these loading programs. In these cases, macro-spin does not develop and the peak stress state corresponds to $f_s(\mathcal{L}:\dot{\boldsymbol{\varepsilon}} - f_d\mathbf{N}||\dot{\boldsymbol{\varepsilon}}||) = \mathbf{0}$, which yields

$$\dot{\boldsymbol{\varepsilon}} = f_d\mathcal{L}^{-1}:\mathbf{N}, \tag{50}$$

where $\dot{\boldsymbol{\varepsilon}} = \dot{\boldsymbol{\varepsilon}}/\|\dot{\boldsymbol{\varepsilon}}\|$ is the normalized strain rate. Since $||\dot{\boldsymbol{\varepsilon}}|| = 1$, the following condition for the peak stresses is obtained:

$$\Phi_p(\hat{\boldsymbol{\sigma}}) = (\mathcal{L}^{-1}:\mathbf{N}):(\mathcal{L}^{-1}:\mathbf{N}) = 1/f_d^2. \tag{51}$$

Herein Φ_b is a function of $\hat{\boldsymbol{\sigma}}$ (or $\hat{\boldsymbol{\sigma}}^d$) only. Note that this peak stress state representation is also relevant to the micro-polar hypoplastic model if couple stress and micro-curvature rate are zero. Given the representations for $\mathcal{L}$ and $\mathbf{N}$ in (13), $\mathcal{L}^{-1}$ and $\Phi_b(\hat{\boldsymbol{\sigma}})$ become

$$\mathcal{L}^{-1} = \frac{1}{\hat{a}^2}\mathcal{I} - \frac{\hat{\boldsymbol{\sigma}}\otimes\hat{\boldsymbol{\sigma}}}{\hat{a}^2(\hat{a}^2 + ||\hat{\boldsymbol{\sigma}}||^2)}, \tag{52}$$

$$\Phi_p(\hat{\boldsymbol{\sigma}}) = \frac{1}{\hat{a}^2}[\eta^2||\hat{\boldsymbol{\sigma}}||^2 + (2\eta+1)||\hat{\boldsymbol{\sigma}}^d||^2] \tag{53}$$

with $\eta = (\hat{a}^2 - ||\hat{\boldsymbol{\sigma}}^d||^2)/(\hat{a}^2 + ||\hat{\boldsymbol{\sigma}}||^2)$.

It can be seen in Equation (51) that the peak state is influenced by the density through the factor f_d. In the vicinity of the peak state, $f_d < 1$ holds. For a loading program starting from an isotropic (hydrostatic) state, numerical tests show that f_d normally falls within a range of $(0{\cdot}85, 1{\cdot}0)$ around the peak state. A geometric representation of the peak state can be presented in a deviatoric stress plane by searching the radial and circumferential directions for points at which (51) is satisfied (refer to Figure 3a). The peak stress states in the deviatoric stress plane for some assumed values for f_d are shown in Figure 3b. The closed loop represents an intersection of the conical peak surface with the deviatoric stress plane. It can be seen that a decrease in the value of f_d corresponds to an expansion of the peak state loop. A value $f_d = 1$ corresponds to stationary states with $\dot{e} = 0$, at which (51) is reduced to $\|\hat{\boldsymbol{\sigma}}^d\| = \hat{a}$. Starting from the same initial relative density, f_d can be closer to 1 for the peak state at a higher mean pressure level. Therefore, the generatrix of the peak state cone is slightly curved, rather than linear, in the meridional plane.

5.2. Bifurcation states versus peak stress states

Now we consider whether bifurcation states will be encountered before the peak stress states are reached. We search the stress states in the deviatoric stress plane by starting from the hydro-static pressure axis and increasing the radius in the deviatoric stress plane, while keeping the Lode angle and the mean pressure constant (refer to Figure 3a). At each point, the bifurcation criteria (30) and (46) and the peak state condition (51) are checked.

In the numerical search algorithm, a maximization procedure is employed to obtain the maximum value of the functions $f_d^2\Phi_0 - 1$ and $f_d^2\Phi_1^* - 1$ for all possible bifurcation directions

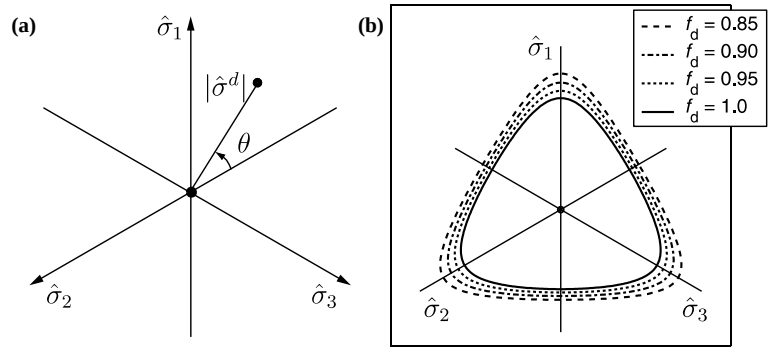

Figure 3. Representation of peak stress on the deviatoric stress plane.

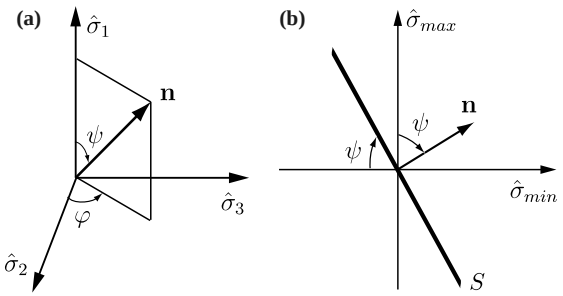

Figure 4. Determination of the direction for the weak discontinuity plane.

defined by the vector $\mathbf{n} = [\cos\psi, \sin\psi\cos\varphi, \sin\psi\sin\varphi]$ (refer to Figure 4). Numerical results, presented in Figure 5, compare the bifurcation points with the peak stress points in the deviatoric stress plane for a constant value $f_d = 0{\cdot}85$ (Figure 5a) and $f_d = 1{\cdot}0$ (Figure 5b).

It can be seen that the peak stress points and the bifurcation points for the non-polar continuum and the micro-polar continuum form three closed loops in the deviatoric stress plane. They are three-fold symmetric or periodic at the Lode angle increment $\Delta\theta = 120^\circ$. The loop of bifurcation points for the non-polar continuum intersects with the peak stress loop, whereas the loop of bifurcation points for the micro-polar continuum lies completely outside the peak stress loop. It should be noted that f_d is not a constant in a real loading program. In the vicinity of the peak states, f_d is increasing as a result of dilation and has a value less than

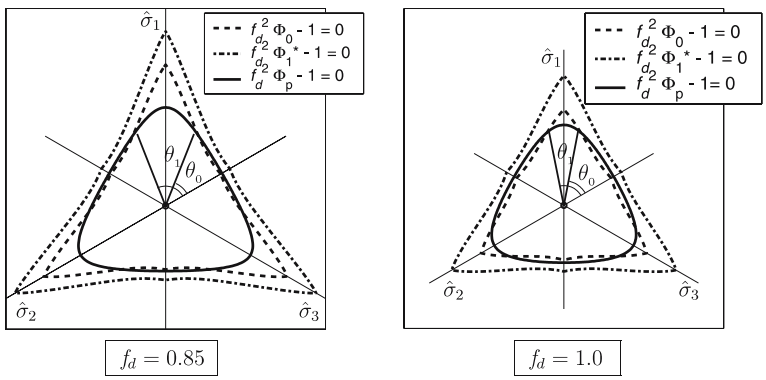

Figure 5. Representation of peak stress points (solid curves) and bifurcation points (dashed and dash-dotted curves) on the deviatoric stress plane.

1·0. Since an increase in f_d corresponds to a shrinking of the peak state and the bifurcation loops, the distance between the bifurcation points and the peak point in an arbitrary direction may be smaller. However, in the specific directions where the bifurcation point coincides with the peak point, f_d must have a unique value at this point. Therefore, the relative positions of these loops are correctly shown in Figure 5.

Bearing in mind that only stress states inside the peak stress loop are accessible, we can interpret these results as follows. In the non-polar continuum, shear bifurcation may occur before the peak state is reached for stress paths with a Lode angle $\theta \in [0, \theta_0)$ and $\theta \in (\theta_1, 120°]$. For stress paths with $\theta \in (\theta_0, \theta_1)$, which includes the stress path for a triaxial compression test, the peak state is reached before bifurcation. This indicates that a homogeneous loading will lead to a homogeneous failure or peak failure rather than a localized failure. A similar result was also obtained in [26] with an amorphous hypoplastic model (*i.e.*, a hypoplastic model with the Cauchy stress being the only state variable).

In contrast to the possible shear bifurcation in the non-polar continuum, Figure 5 shows that no bifurcation point will be reached before the peak state in the micro-polar continuum, even though the bifurcation states lie close to the peak states for a smaller Lode angle. This result means that there is no solution for the discontinuity vector $\mathbf{g}^u$ within the accessible stress domain (which is an area in the principal stress space surrounded by a cone-shaped peak-stress surface with its apex at the origin), which indicates that only homogeneous failure or peak failure will occur in a homogeneously deforming continuum body. As no restriction has been put on vector $\mathbf{g}^u$, the result also rules out a co-axial solution of $\mathbf{g}^u$ with respect to $\mathbf{n}$. In other words, pure compression or tension localization is excluded too. In an earlier analysis of localized failure with a micropolar elastoplastic model, Iordache and Willam [27] found that the micropolar continuum description suppresses localization bifurcation in shear. It may not suppress localization bifurcation in pure tension. This is, however, not in contradiction with our results, since the micropolar hypoplastic model used in this study is defined only in a compressive sub-domain in the principal stress space, as a cohesionless granular material can not sustain tension. While localized failure is widely observed experimentally in biaxial compression tests [31,32], peak failures have also been observed in triaxial compression tests [33] and in true triaxial tests [34]. It should be pointed out that in the bifurcation analysis, ideally homogeneous states are assumed in the continuum. However, in a real granular medium some packing inhomogeneity is inevitable. On the micro-scale, the void ratio varies significantly from point to point even though a macroscopically homogeneous condition is maintained. Shahinpoor [35] showed that even within a granular body composed of equal-sized spheres, the void ratio or porosity will not be uniform. This inhomogeneity of the void ratio can lead to a fluctuation in stress as well on the micro-scale when a granular specimen is loaded uniformly on its boundary. Numerical results have shown that such a state fluctuation is sufficient to initiate shear localization in a granular specimen undergoing a uniform loading process [36,37]. Therefore, in the micro-polar hypoplastic description, shear localization may occur, not in the form of sudden shear bifurcation, but rather in the form of continuous development of deformation inhomogeneity as a result of state fluctuation and strain softening.

For the non-polar continuum, the intersection points of the bifurcation and the peak state loops vary with respect to f_d (Figure 5). This result can be explained by the density-dependence of the inclination of the weak discontinuity plane. The latter, which is defined by the angles φ and ψ (refer to Figure 4), varies not only with the Lode angle θ but also with the

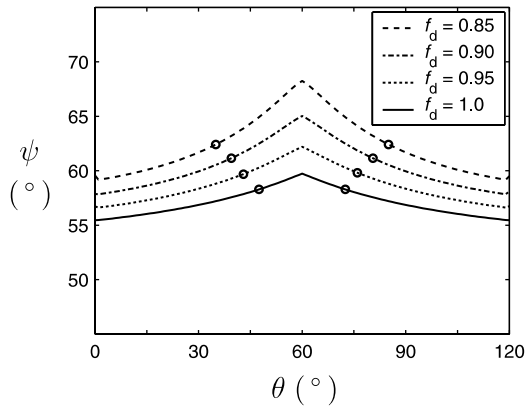

Figure 6. Inclination of the weak discontinuity plane in the non-polar hypoplastic continuum.

density factor f_d. Numerical results for the non-polar continuum show that

$$\varphi = \begin{cases} 180^\circ \text{ for } \theta \in [0, 60^\circ), \\ 90^\circ \quad \text{for } \theta \in (60^\circ, 120^\circ] \end{cases}$$

which means that the weak discontinuity plane has its normal perpendicular to the intermediate principal stress direction. In other words, the weak discontinuity will occur in the plane defined by the maximum and minimum principal stresses. The inclination of the discontinuity plane is, however, influenced by the intermediate principal stress since ψ varies with the variation of the Lode angle θ (Figure 6). An increase in the inclination of the discontinuity plane is obtained for a smaller value for f_d. The intersection points between the bifurcation loop and the peak loop are marked in Figure 6. Between these marks a homogeneous failure is predicted.

6. Conclusion

Shear localization in granular materials has been studied at the constitutive model level as a bifurcation problem. The materials have been modelled as a non-polar continuum and as a micro-polar continuum using a hypoplastic description. The bifurcation conditions have been formulated in a general manner for the two incrementally nonlinear constitutive models. These conditions indicate that shear bifurcation depends on the stress and density state in the non-polar continuum and on the couple stress state as well in the micro-polar continuum. The possibility of shear localization has been examined using a geometric interpretation for the bifurcation states and the peak stress states in the principal stress space. The peak stress states form a conical surface in the principal stress space bounding the accessible stress domain. The stress states for bifurcation have been identified on the deviatoric stress plane and compared with the peak stress states. The results show that, in the non-polar hypoplastic continuum, weak discontinuity bifurcation will occur in certain loading paths, whereas in the micro-polar hypoplastic continuum, weak discontinuity bifurcation will never occur.

In the non-polar continuum description of material behaviour, occurrence of shear localization is often attributed to the weak discontinuity bifurcation, a mathematical property associated with the constitutive models of this type. The bifurcation analyses for the micro-polar hypoplastic continuum in this work and for a micro-poplar elastoplastic continuum by Iordache and Willam suggest that the property of weak discontinuity bifurcation may no longer

be associated with a micro-polar constitutive model. And shear localization at the constitutive model level may generally be suppressed in the micro-polar continuum description of material behaviour. While shear localization has been widely observed in experiments and engineering practice, this physical phenomenon now can be interpreted as only a result of structure response. The inhomogeneity at the micro-structure level, the inevitably existing state fluctuation and the strain softening are the main causes leading to shear localization in a homogeneous-on-the-macro-level granular body.

Acknowledgement

The financial support by Australia Research Council (grant DP0453056) is acknowledged by the first author.

Appendix A

Let $\mathbf{A}$ be a partitioned square matrix in the form of

$$\mathbf{A}=\begin{bmatrix}\mathbf{A}_{11} & \mathbf{A}_{12}\\ \mathbf{A}_{21} & \mathbf{A}_{22}\end{bmatrix}.$$

If $\mathbf{A}$ is invertible, its inverse

$$\mathbf{B}=\mathbf{A}^{-1}=\begin{bmatrix}\mathbf{B}_{11} & \mathbf{B}_{12}\\ \mathbf{B}_{21} & \mathbf{B}_{22}\end{bmatrix}$$

can be obtained by

$$\mathbf{B}_{22}=(\mathbf{A}_{22}-\mathbf{A}_{21}\cdot\mathbf{A}_{11}^{-1}\cdot\mathbf{A}_{12})^{-1},$$

$$\mathbf{B}_{12}=-\mathbf{A}_{11}^{-1}\cdot\mathbf{A}_{12}\cdot\mathbf{B}_{22},$$

$$\mathbf{B}_{21}=-\mathbf{B}_{22}\cdot\mathbf{A}_{21}\cdot\mathbf{A}_{11}^{-1},$$

$$\mathbf{B}_{11}=\mathbf{A}_{11}^{-1}-\mathbf{B}_{12}\cdot\mathbf{A}_{21}\cdot\mathbf{A}_{11}^{-1}.$$

This representation shows that the invertibility of $\mathbf{A}$ depends on $\mathbf{A}_{11}$ and $\mathbf{A}_{22}-\mathbf{A}_{21}\cdot\mathbf{A}_{11}^{-1}\cdot\mathbf{A}_{12}$ being invertible. If $\mathbf{A}$ stands for $\mathbf{\Pi}$ and we neglect the terms $\mathbf{P}''_{uu}$ and $\mathbf{P}''_{wu}$ for $p << f_{\mathrm{s}}$, we have

$$\mathbf{A}_{11}=\mathbf{P}'_{uu},\ \mathbf{A}_{12}=\mathbf{P}_{uw},\ \mathbf{A}_{21}=\mathbf{P}'_{wu},\ \mathbf{A}_{22}=\mathbf{P}_{ww}.$$

Referring to expression (37), $\mathbf{A}_{11}$ and $\mathbf{A}_{22}$ are basically invertible. In particular,

$$\mathbf{A}_{11}^{-1}=\frac{1}{\hat{a}^2}\left(\mathbf{I}-\frac{\hat{\mathbf{t}}_n\otimes\hat{\mathbf{t}}_n}{\hat{a}^2+\|\hat{\mathbf{t}}_n\|^2}\right),$$

where $\hat{\mathbf{t}}_n=\hat{\boldsymbol{\sigma}}\cdot\mathbf{n}$ denotes the normalized traction on plane S. Furthermore, by inserting all components in this expression, the following representation can be obtained:

$$\mathbf{A}_{22}-\mathbf{A}_{21}\cdot\mathbf{A}_{11}^{-1}\cdot\mathbf{A}_{12}=d_{50}\left[a_{\mu}^2\mathbf{I}+\left(1-\frac{1}{\hat{a}^2+\|\hat{\mathbf{t}}_n\|^2}\right)\hat{\mathbf{m}}_n\otimes\hat{\mathbf{m}}_n\right],$$

where $\hat{\mathbf{m}}_n=\hat{\boldsymbol{\mu}}\cdot\mathbf{n}$ denotes the normalized couple traction on plane S. Obviously $\mathbf{A}_{22}-\mathbf{A}_{21}\cdot\mathbf{A}_{11}^{-1}\cdot\mathbf{A}_{12}$ is invertible, too.

References

1. J.R. Rice, The localization of plastic deformation. In: W.T. Koiter (ed.), *Theoretical and Applied Mechanics*. North-Holland Publishing Company, Amsterdam (1976) pp. 207–220.
2. J.W. Rudnicki and J.R. Rice, Conditions for the localization of deformation in pressure-sensitive dilatant materials. *J. Mech. Phy. Solids* 23 (1975) 371–394.
3. I. Vardoulakis, Bifurcation analysis of the plane rectilinear deformation on dry sand sample. *Int. J. Solids Struct.* 17 (1981) 1085–1101.
4. N.S. Ottosen and K. Runesson, Properties of discontinuous bifurcation solutions in elasto-plasticity. *Int. J. Solids Struct.* 27 (1976) 401–421.
5. J.P. Bardet and I. Vardoulakis, The asymmetry of stress in granular media. *Int. J. Solids Struct.* 38 (2001) 353–367.
6. W. Ehlers, E. Ramm, S. Diebels and G.A. D'Addetta, From particle ensembles to Cosserat contiua: homogenization of contact forces towords stress and couple stresses. *Int. J. Solids Struct.* 40 (2003) 6681–6702.
7. H.-B. Mühlhaus, Scherfugenanalyse bei granularem Material in Rahmen der Cosserat-Theorie. *Ingenieur-Archiv* 56 (1986) 389–399.
8. R. de Borst, Simulation of strain localization: a reappraisal of the Cosserat-continuum. *Engng. Comp.* 8 (1991) 317–332.
9. A. Dietsche, P. Steinmann and K.J. Willam, Micropolar elasto-plasticity and its role in localization analysis. *Int. J. Plast.* 9 (1993) 813–831.
10. W. Ehlers and W. Volk, On theoretical and numerical methods in the theory of porous media based on polar and non-polar solid materials. *Int. J. Solids and Struct.* 35 (1998) 4597–5616.
11. J. Tejchman, Modelling of shear localisation and autogeneous dynamic effects in granular bodies. *Veröffentlichungen des Institutes für Bodenmechanik und Felsmechanik der Universität Fridericiana in Karlsruhe*, Heft 140 (1997).
12. J. Tejchman and E. Bauer, Numerical simulation of shear band formation with a polar hypoplastic model. *Comp. Geotech.* 19 (1996) 221–244.
13. E. Bauer and W. Huang, Numerical study of polar effects in shear zones. In: Pande and Pietruszczak and Schweiger (eds.), *Numerical Models in Geomechanics–NUMOG VII*. Rotterdam: A.A. Balkema (1999) pp. 133–138.
14. J. Tejchman and G. Gudehus, Shearing of a narrow granular layer with polar quantities. *Int. J. Numer. Anal. Meth. Geomech.* 25 (2001) 1–28.
15. W. Huang and E. Bauer, Numerical investigations of shear localization in a micro-polar hypoplastic material. *Int. J. Numer. Anal. Meth. Geomech.* 5 (2003) 124–148.
16. G. Gudehus, A comprehensive constitutive equation for granular materials. *Soils Found.* 36 (1996) 1–12.
17. E. Bauer, Calibration of a comprehensive hypoplastic model for granular materials. *Soils Found.* 36 (1996) 13–26.
18. W. Huang, K. Nübel and E. Bauer, Polar extension of a hypoplastic model for granular materials with shear localization. *Mech. Mat.* 34 (2002) 563–576.
19. D. Kolymbas, Bifurcation analysis for sad samples with a non-linear constitutive equation. *Ingenieur-Archiv* 50 (1981) 131–140.
20. R. Chambon and J. Desrues, Bifurcation par localisation et non linéarité incrémentale: un example heuristique d'analyse complété. In: *Plasticity Instability*. Paris: Press ENPC. (1985) pp. 101–119.
21. J. Desrues and R. Chambon, Shear band analysis for granular materials: The question of incremental non-linearity. *Ingenieur-Archiv* 59 (1989) 187–196.
22. R. Chambon, S. Crochepeyer and J. Desrues, Localization criteria for non-linear constitutive equations of geomaterials. *Mech. Cohesive-Fric. Mater.* 5 (2000) 61–82.
23. E. Bauer and W. Huang, The dependence of shear banding on pressure and density in hypoplasticity. In: Adachi, Oka and Yashima (eds.), *Localization and Bifurcation Theory for Soils and Rocks*. Rotterdam: A.A. Balkema (1998) pp. 81–90.
24. E. Bauer, Analysis of shear band bifurcation with a hypoplastic model for a pressure and density sensitive granular mateiral. *Mech. Mater.* 31 (1999) 597–609.
25. W. Wu and Z. Sikora, Localized bifurcation in hypoplasticity. *Int. J. Engng. Sci.* 29 (1991) 195–201.
26. W. Wu, Non-linear analysis of shear band formation in sand. *Int. J. Numer. Anal. Meth. Geomech.* 24 (2000) 245–263.

27. M.-M. Iordache and K. Willam, Localized failure analysis in elastoplastic Cosserat continua. *Comput. Methods Appl. Mech. Engng.* 151 (1998) 559–586.
28. E. Bauer, Conditions for embedding Casagrande's critical states into hypoplasticity. *Mech. Cohesive-Frict. Mater.* 5 (2000) 124–148.
29. I. Herle and G. Gudehus, Determination of parameters of a hypoplastic constitutive model from properties of grain assemblies.. *Mech. Cohesive-Fric. Mater.* 4 (1999) 461–486.
30. G.A. Holzapfel, *Nonlinear Solid Mechanics–A Continuum Approach for Engineering*. Chichester: John Wiley (2001) 455 pp.
31. I. Vardoulakis and B. Graf, Calibration on constitutive models for granular materials using data from biaxial experiments. *Géotechnique* 35 (1985) 299–317.
32. D. Mokni and J. Desrues, Strain localization measurements in undrained plane-strain biaxial tests on Hostun RF sand. *Mech. Cohesive-Fric. Mater.* 4 (1998) 419–441.
33. P.V. Lade, Localization effects in triaxial tests on sand. In: Proc. IUTAM Symposium on *Deformation and Failure of Granular Materials*, Delft (1982) pp. 461–471.
34. Q. Wang and P.V. Lade, Shear banding in true triaxial tests and its effect on failure in sand. *ASCE J. Engng. Mech.* 127 (2001) 754–761.
35. M. Shahinpoor, Statistical mechanical considerations on storing bulk solids. *Bulk Solids Handling* 1 (1981) 31–36.
36. K. Nübel, Experimental and numerical investigation of shear localization in granular material. *Veröffentlichungen des Institues für Bodenmechanik und Felsmechanik der Universität Fridericiana in Karlsruhe*, Heft 159 (2003) 159 pp.
37. K. Nübel and W. Huang, A study of localized deformation pattern in granular media. *Compt. Meth. Appl. Mech. Engng.* 193 (2004) 2719–2743.